Human Molecular Genetics, 2013, Vol. 22, No. 21 ***4417–4429***
doi:10.1093/hmg/ddt292
Advance Access published on June 27, 2013

Muscle-specific function of the centronuclear myopathy and Charcot–Marie–Tooth neuropathy-associated dynamin 2 is required for proper lipid metabolism, mitochondria, muscle fibers, neuromuscular junctions and peripheral nerves

Elisa Tinelli, Jorge A. Pereira and Ueli Suter*

Department of Biology, Institute of Molecular Health Sciences, Cell Biology, Swiss Federal Institute of Technology, ETH Zurich, Zurich 8093, Switzerland

Received April 29, 2013; Revised and Accepted June 19, 2013

The ubiquitously expressed large GTPase Dynamin 2 (DNM2) plays a critical role in the regulation of intracellular membrane trafficking through its crucial function in membrane fission, particularly in endocytosis. Autosomal-dominant mutations in *DNM2* cause tissue-specific human disorders. Different sets of *DNM2* mutations are linked to dominant intermediate Charcot–Marie–Tooth neuropathy type B, a motor and sensory neuropathy affecting primarily peripheral nerves, or autosomal-dominant centronuclear myopathy (CNM) presenting with primary damage in skeletal muscles. To understand the underlying disease mechanisms, it is imperative to determine to which degree the primary affected cell types require DNM2. Thus, we used cell type-specific gene ablation to examine the consequences of DNM2 loss in skeletal muscle cells, the major relevant cell type involved in CNM. We found that DNM2 function in skeletal muscle is required for proper mouse development. Skeletal muscle-specific loss of DNM2 causes a reduction in muscle mass and in the numbers of muscle fibers, altered muscle fiber size distributions, irregular neuromuscular junctions (NMJs) and isolated degenerating intramuscular peripheral nerve fibers. Intriguingly, a lack of muscle-expressed DNM2 triggers an increase of lipid droplets (LDs) and mitochondrial defects. We conclude that loss of DNM2 function in skeletal muscles initiates a chain of harmful parallel and serial events, involving dysregulation of LDs and mitochondrial defects within altered muscle fibers, defective NMJs and peripheral nerve degeneration. These findings provide the essential basis for further studies on DNM2 function and malfunction in skeletal muscles in health and disease, potentially including metabolic diseases such as diabetes.

INTRODUCTION

Multiple autosomal-dominant missense and short deletion mutations have been identified in the *Dynamin 2 (DNM2)* locus. Distinct groups of mutations are associated with dominant intermediate Charcot–Marie–Tooth neuropathy type B (DI-CMTB) or autosomal-dominant centronuclear myopathy (CNM) (1,2). While DI-CMTB affects axons and myelinating Schwann cells of peripheral nerves, CNM caused by mutations in *DNM2* (DNM2-CNM) is characterized by slowly progressive muscular weakness with abnormal centralization of nuclei in myofibers, radial arrangement of sarcoplasmic strands, type I fiber predominance and small fiber sizes (3,4). How the different DNM2 mutant proteins lead to distinct diseases, affecting different cell types as specific primary targets, is largely unclear. In DI-CMTB, defective endocytosis is likely to be critical (2), while impairment of autophagy might be a significant contributor in DNM2-CNM (5). Special effects on flawed membrane remodeling may be a common underlying feature (6). A major progress on these crucial issues is expected to come from

*To whom correspondence should be addressed at: Institute of Molecular Health Sciences, ETH Hönggerberg, CH-8093 Zürich, Switzerland. Tel: +41 446333432; Fax: +41 446331328; Email: ueli.suter@biol.ethz.ch

improved understanding of the normal physiological function of DNM2 and its malfunctions in disease, on the molecular, cellular, tissue, organ and organism levels.

Molecularly, DNM2 belongs to the classical dynamins comprising DNM1 (mainly expressed by neurons), DNM2 (ubiquitously expressed) and DNM3 (expressed mainly in brain and testes) (7). These cytosolic proteins are large GTPases that act mechano-chemically to mediate membrane fission. At the cellular level related to this function, classical dynamins regulate a plethora of crucial processes, including endocytosis and intracellular membrane trafficking in an interplay with the cytoskeleton. Extensive work has provided a wealth of information on the structure–function relationship of dynamins (7,8). Classical dynamins have a well-conserved N-terminal GTPase domain, a middle domain (MD) important for oligomerization and a pleckstrin-homology (PH) domain that binds phosphoinositides, followed by a GTPase effector domain. The C-terminal proline-rich domain coordinates dynamin function by physically interacting with various SH3 domain-containing proteins. DNM2 mutations associated with DI-CMTB are clustered in the N-terminal part of the PH domain, while DNM2-CNM mutations are predominantly found in the C-terminal region of the same domain and in the MD (2,5). Biochemically, altered GTPase activity (9) and formation of abnormally stable polymers have been reported for some DNM2-CNM mutants (10). In contrast, selected CMT-associated DNM2 mutants show reduced binding to membranes (11).

On the tissue level and in organisms, mouse models carrying a *Dnm2*-CNM mutation [Knock-in R465W (1,5)], or viral-vector-mediated overexpression of DNM2 wild-type or the R456 mutant proteins (12), revealed variable muscle dysfunctions associated with mitochondrial, proteasomal and autophagy defects. Consistent with these data, mice lacking miRNA 133a and consequently overexpressing its Dnm2 target, developed a CNM-like phenotype (13). Expression knockdown of *dnm2* and *dnm2-like*, the putative *DNM2* orthologs in zebrafish, resulted in extensive morphological abnormalities during development (14).

We found that mice carrying a ubiquitous heterozygous deletion of *Dnm2* have no detectable phenotype up to the age of 15 months, the last time point examined (unpublished data). These results strongly indicate that disease-causing DNM2 mutations (these mutations are all dominantly inherited) are not loss-of-function mutations causing disease due to DNM2 haploinsufficiency, but rather act by gain-of-function or dominant-negative mechanisms. This raises the important question whether skeletal muscles are fundamentally dependent on DNM2 function. We tested this issue using ablation of *Dnm2* specifically in mouse skeletal muscles. Our data show that DNM2 function in muscle is strictly required for proper mouse development.

RESULTS

DNM2 function in skeletal muscle is required for proper mouse development

In this study, we have used a conditional mouse null allele for *Dnm2* ($Dnm2^{fl}$) that was generated by flanking exon 2 with *LoxP* sites using homologous recombination and standard embryonic stem cell technology (2). To assess whether DNM2 function in skeletal muscle is required for proper mouse development, we bred mice carrying the $Dnm2^{fl}$ allele with an established mouse line that expresses Cre recombinase specifically in skeletal muscle cells [HSACre (15)]. The experimental breeding ($HSACre\ Dnm2^{fl/+} \times Dnm2^{fl/fl}$) yielded the expected genotypes in the Mendelian ratio. To confirm tissue-specific loss of DNM2 in $HSACreDnm2^{fl/fl}$ mice, we analyzed protein lysates from gastrocnemius muscle at postnatal day (P) 5 and P10 by western blotting. As expected, DNM2 levels were strongly reduced in $HSACreDnm2^{fl/fl}$ mutants compared with control lysates (Fig. 1A). Residual amounts of DNM2 are likely mainly due to DNM2-expressing, non-targeted muscle-resident cells including Schwann cells, fibroblasts and satellite cells. Next, we reasoned that other functionally similar members of the classical dynamin protein family might be aberrantly regulated in the absence of DNM2 as part of potential compensatory mechanisms. In line with this hypothesis, we found that DNM1 expression was increased in $HSACreDnm2^{fl/fl}$ mice-derived gastrocnemius muscle lysates compared with controls, both at P5 and at P10, while DNM3 levels were not altered (Fig. 1A).

$HSACreDnm2^{fl/fl}$ mice were generally weaker than their littermates and became moribund between P11 and P14. We found that the body weight of $HSACreDnm2^{fl/fl}$ mutants was significantly decreased compared with controls already at P5 and even more strikingly at P10 (Fig. 1B and E). Determining the ratios between the weight of the gastrocnemius muscle or the diaphragm muscle and the body weight revealed significant reductions at P5 and P10 in mutants versus controls (Fig. 1C and D), consistent with loss of muscle mass. Qualitative inspections revealed a similarly decreased mass of other muscles, including the gluteus muscle, the tibialis muscle and the quadriceps muscle.

Skeletal muscles are dependent on DNM2 function

The observed decrease in the muscle mass of $HSACreDnm2^{fl/fl}$ mice suggests a skeletal muscle defect. The main factors that may contribute to this finding are muscle fiber loss, muscular hypotrophy or atrophy and/or a delay in muscle development. To address this issue, we examined first the muscle morphology on hematoxylin/eosin-stained cross-sections of gastrocnemius muscles. Already at P5, the muscles of $HSACreDnm2^{fl/fl}$ mice were grossly abnormal (Fig. 2A). Mutant muscle fibers appeared to be slightly larger than in control mice, defective fibers were present and the interstitial space was enlarged, leaving the impression of a decreased muscle fiber density compared with controls. At P10, damaged muscle fibers dominated in $HSACreDnm2^{fl/fl}$ mice, and Masson trichrome staining revealed a minor increase in collagen compared with controls (Supplementary Material, Fig. S1).

To address whether the altered morphology results from aberrant cell survival and/or from a delay in muscle cell maturation, we analyzed first cell death and cell proliferation. TUNEL assays on cross-sections of P5 and P10 gastrocnemius muscles from $HSACreDnm2^{fl/fl}$ mice and controls revealed increased cell death in mutants at both time points (Fig. 2B). Parallel proliferation analyses using short-term BrdU injections and appropriate staining techniques revealed a modest increase in cell proliferation in $HSACreDnm2^{fl/fl}$ mice compared with controls at P5,

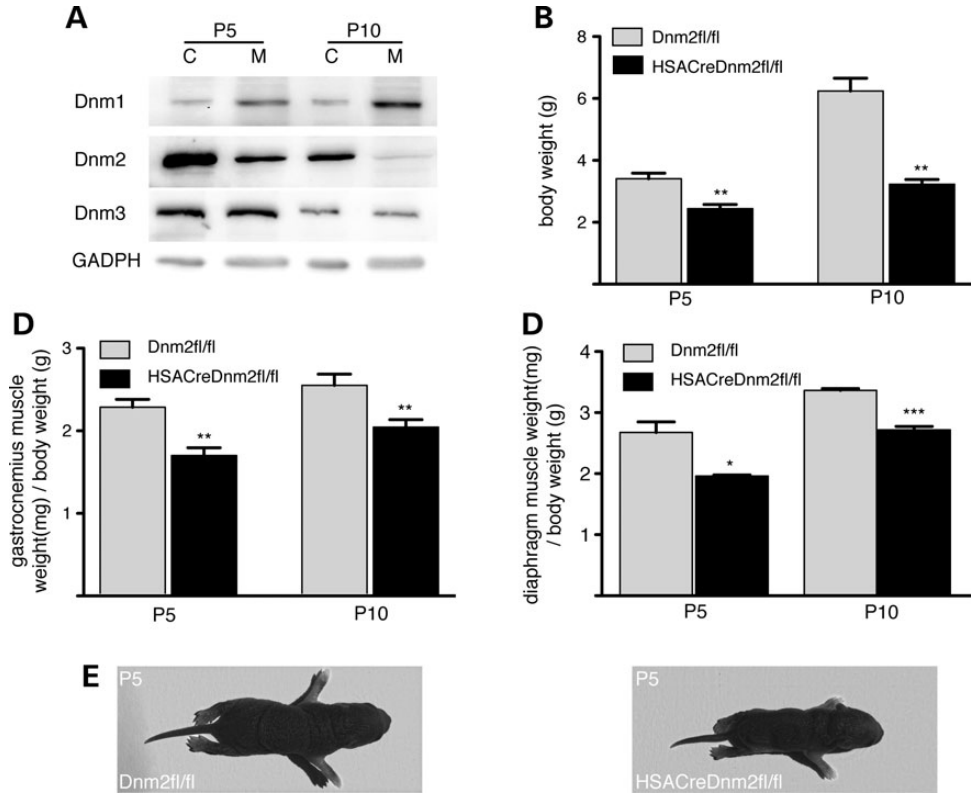

Figure 1. Ablation of DNM2 in skeletal muscles impedes normal mouse development due to reduced muscle mass. (**A**) Western blot analysis of expression levels of classical dynamins in gastrocnemius muscles of HSACreDnm2$^{fl/fl}$ mutant mice (M) and Dnm2$^{fl/fl}$ controls (C) at P5 and P10. In mutant animals compared with controls, Dnm2 levels are reduced, Dnm1 is upregulated and Dnm3 expression is not altered. GAPDH served as a loading control. A representative blot out of five independent experiments is shown. (**B**) Quantitative analysis of body weights in grams (g) of HSACreDnm2$^{fl/fl}$ and Dnm2$^{fl/fl}$ mice at P5 and P10 showing reduced body weights of mutant animals compared with controls. (**C**) Analysis of the ratio between gastrocnemius muscle weight in milligrams (mg) and body weight in grams (g) of HSACreDnm2$^{fl/fl}$ mutant mice and Dnm2$^{fl/fl}$ controls at P5 and P10 revealing reductions in mutants compared with controls, consistent with reduced muscle mass. (**D**) Analysis of the ratio between diaphragm muscle weight in milligrams (mg) and body weight in grams (g) of HSACreDnm2$^{fl/fl}$ mutant mice and Dnm2$^{fl/fl}$ controls at P5 and P10 shows reductions in mutants compared with controls, consistent with the reduced muscle mass. At least 14 animals of each genotype and developmental age were included in the analyses in (B) and (C). Three animals per genotype and developmental age were included in the analyses in (D). (**E**) Representative pictures of HSACreDnm2$^{fl/fl}$ mutant mice and Dnm2$^{fl/fl}$ controls at P5; $^{*}P < 0.05$, $^{**}P < 0.01$, $^{***}P < 0.001$.

contrasting with a decrease in proliferation in mutants versus controls at P10 (Fig. 2C).

The observed early changes in cell proliferation and cell death might be interpreted as alterations in the maturation status of muscles lacking DNM2. To examine this matter, we used an anti-developmental myosin heavy chain (dMHC) antibody recognizing embryonic and neonatal MHC isoforms that are downregulated during muscle maturation. Cross-sections of P5 and P10 gastrocnemius muscles of *HSACreDnm2*$^{fl/fl}$ mice and controls were stained for dMHC together with the fiber boundary marker laminin γ1. We found dMHC-positive fibers in both P5 mutant and control muscles without appreciable differences ($8.0 \pm 0.7\%$ in controls and $8.2 \pm 0.9\%$ in mutants, $n = 3$; Fig. 2D). Corresponding western blot analyses revealed comparable dMHC levels in mutant and control mice at both P5 and P10 (Fig. 2E). As expected and validating the antibody reagent, dMHC expression was lower at P10 compared with P5 (16), while total MHC levels remained unchanged.

Based on the results obtained so far, we favored the hypothesis that muscle atrophy and/or fiber loss are major contributors to the pathology observed after loss of DNM2 in skeletal muscle. To address this issue, we analyzed first the total number of muscle fibers on hematoxilin/eosin-stained cross-sections of gastrocnemius muscles from P5 and P10 *HSACreDnm2*$^{fl/fl}$ mice and controls. We found a decrease in the number of muscle fibers in mutants compared with controls at both time points (Fig. 3A). In the second step, we performed the corresponding ultrastructural analysis to evaluate muscle fiber size distributions. As suggested previously by the hematoxilin/eosin staining (Fig. 2A), a shift toward larger muscle fiber calibers was found in *HSACreDnm2*$^{fl/fl}$ mice in comparison to controls at P5 (Fig. 3B). In contrast at P10, we detected an increase in the proportion of small caliber muscle fibers in *HSACreDnm2*$^{fl/fl}$ mice (Fig. 3C). We conclude that *Dnm2* ablation in skeletal muscle causes alterations in fiber size, fiber atrophy and fiber loss.

Lack of DNM2 in skeletal muscles causes dysregulation of LDs

Ultrastructural analysis of the gastrocnemius muscle of *HSACreDnm2*$^{fl/fl}$ mice and controls revealed aberrant regulation of lipid droplets (LDs) in mutants. Such droplets serve as stores of metabolic energy and membrane components, regulate various cellular processes, and are linked to several pathological

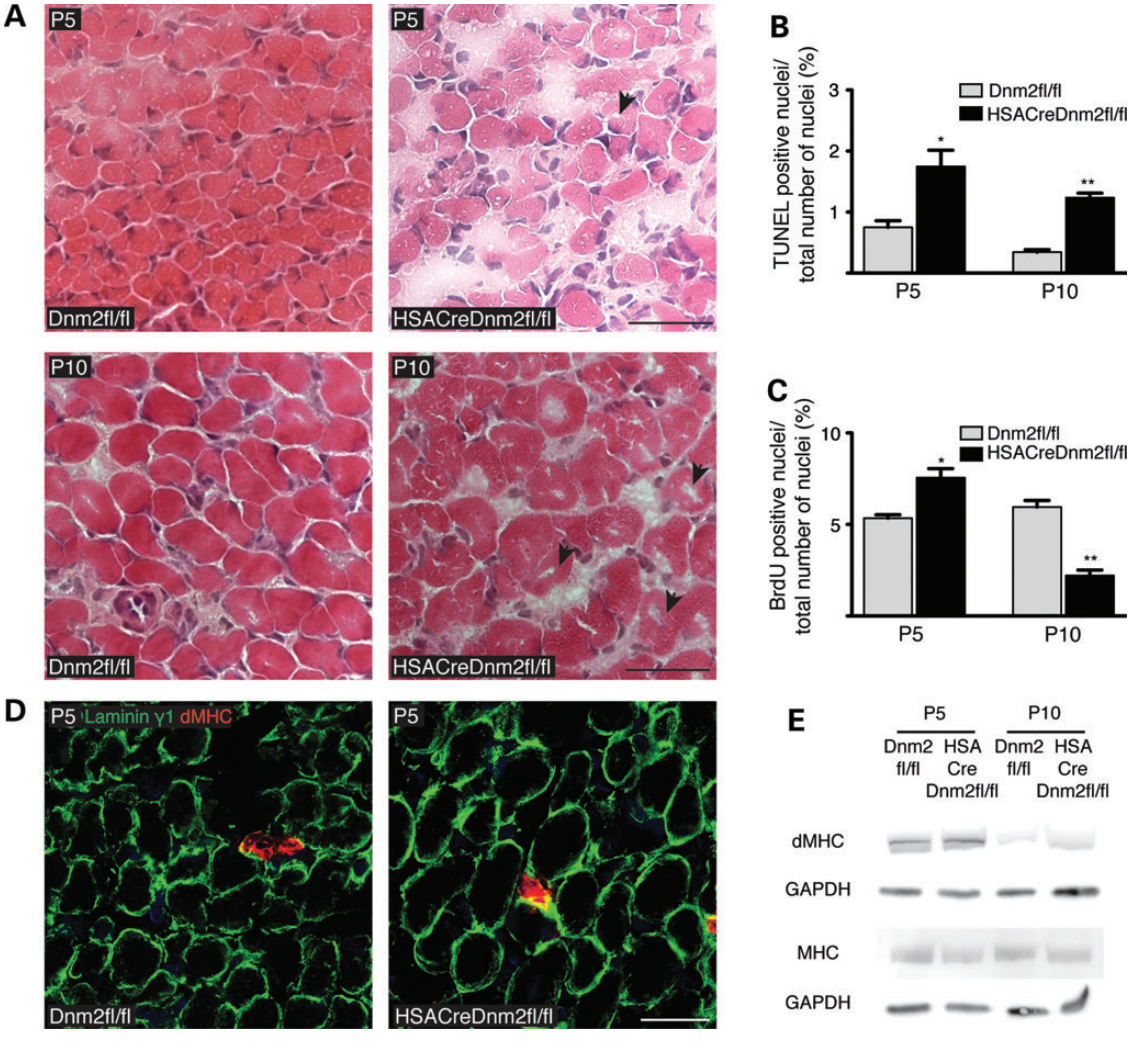

Figure 2. Deficient structures, increased cell death and altered proliferation in muscles lacking DNM2. (**A**) Hematoxylin/eosin stainings of cross-sections of gastrocnemius muscles of HSACreDnm2$^{fl/fl}$ mutant mice and Dnm2$^{fl/fl}$ controls at P5 and P10. Damaged fibers (arrowheads) are plentiful in mutants. At least four animals of each genotype and age have been analyzed and representative pictures are shown. Scale bars = 20 μM. (**B**) Quantification of cell death in gastrocnemius muscle by TUNEL. The ratios between the number of apoptotic cells (TUNEL positive) and total number of nuclei are increased in mutant animals compared with controls at both P5 and P10. (**C**) Proliferation in the gastrocnemius muscle, as determined by the ratio between BrdU-positive nuclei versus total number of nuclei, is increased in mutants compared with control mice at P5 and decreased at P10. In (B) and (C), three animals were analyzed and at least 1000 nuclei per animal counted; $^{*}P < 0.05$, $^{**}P < 0.01$. (**D**) Single-plane confocal microscopy sections of tissue cross-sections of gastrocnemius muscles of P5 mice, stained for laminin γ1 (green) and dMHC(red) expression. A representative picture out of three independent experiments is shown. Scale bar = 25 μM. (**E**) Western blot analysis of dMHC and MHC levels of gastrocnemius muscles shows no differences between mutants and controls at P5 or P10. GAPDH served as a loading control. A representative blot out of four independent experiments is depicted.

conditions (17). At P5, we found both an increased LD density and an increased area that was occupied by LDs in the gastrocnemius muscle of *HSACreDnm2$^{fl/fl}$* mice compared with controls (Fig. 4A and C). These findings were qualitatively confirmed using Oil red O stainings (Fig. 5). In contrast at P10, the density of LDs was decreased in *HSACreDnm2$^{fl/fl}$* gastrocnemius muscles compared with controls (Fig. 4B and D). At this age, the analysis also revealed a trend toward a smaller area occupied by LDs in the mutants, but the difference did not reach statistical significance (Fig. 4D). LDs are often associated with other organelles including endosomes and mitochondria (17). Furthermore, DNM2 regulates various aspects of endosome biology and interacts with the cytoskeleton (7). Thus, we evaluated whether lack of DNM2 influences the position of LDs inside muscle fibers. We counted LDs that did not contact the sarcolemma (inside fiber) and those that contacted the sarcolemma (border fiber). No major differences were found between *HSACreDnm2$^{fl/fl}$* gastrocnemius muscles and controls at P5 and P10, although there was a minor increase in the portion of LDs contacting the sarcolemma at P10 in the mutants (Fig. 4E and F). Furthermore, at P5 we found a significant increase in the density of LDs forming clusters in mutant muscles compared with controls (arrowheads in Fig. 4A, Supplementary Material, Fig. S2).

To characterize the intriguing DNM2-dependent LD alterations further, we evaluated the localization and levels of two proteins. Adipocyte differentiation-related protein (ADRP-adipophilin) was chosen due to its prominent localization to LD membranes

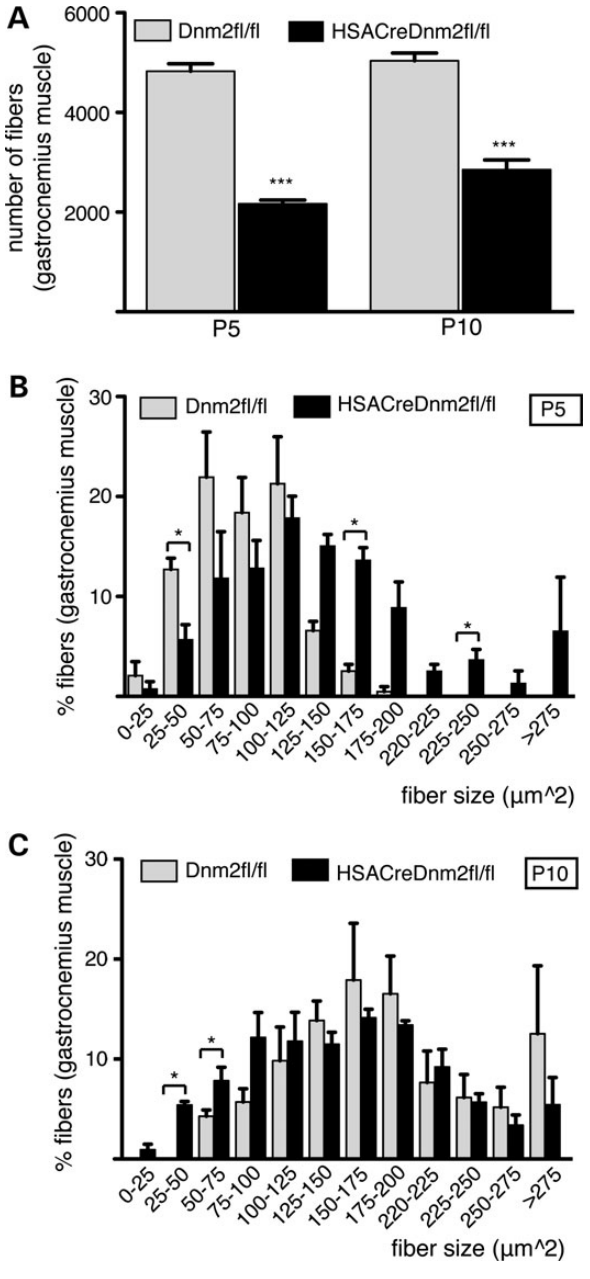

Figure 3. Reduced numbers and altered size distributions of muscle fibers due to DNM2 deficiency. (**A**) Quantitative analysis of fiber numbers of gastrocnemius muscles of HSACreDnm2$^{fl/fl}$ mutant mice and Dnm2$^{fl/fl}$ controls at P5 and P10 reveals decreases in mutants. (**B**) Analysis of fiber distributions in gastrocnemius muscle at P5 and (**C**) at P10 in mutants versus control mice. Note the increase in the portion of large caliber fibers in mutants at P5, while there is an increase in the small caliber fiber portions at P10. Three animals were analyzed for each genotype and developmental age; $^{*}P < 0.05$, $^{***}P < 0.001$.

(18). Caveolin 3 was selected since caveolin can be localized to LDs under various experimental, but also physiological conditions (17). Furthermore, caveolin 3 plays a crucial role in the proper assembly of caveolae at the plasma membrane in skeletal muscle as highlighted by various skeletal muscle diseases due to caveolin 3 defects (limb–girdle muscular dystrophy, rippling muscle disease, distal myopathy and hyperCKemia (19)). Cross-sections of gastrocnemius muscles, collected at P5 and P10 from *HSACreDnm2*$^{fl/fl}$ mice and controls, were stained for adipophilin or caveolin 3 in combination with the fiber boundary marker laminin γ1. Compared with control animals, adipophilin staining was much more abundant within muscle fibers of mutant mice at P5 (Fig. 6A) and remained increased at P10 (Fig. 6B). Consistent with these immunohistochemical findings, western blot analysis revealed that adipophilin protein levels were also increased in mutants compared with controls, both at P5 and at P10 (Fig. 6E). Caveolin 3 staining revealed no particular localization within the core of gastrocnemius muscle fibers of *HSACreDnm2*$^{fl/fl}$ and control mice (Fig. 6C and D). However, caveolin 3 distribution was disorganized at the muscle fiber plasma membrane in mutants (Fig. 6C and D) and caveolin 3 protein levels were increased compared with controls, both at P5 and at P10 (Fig. 6C, D and F). We consider it likely that these findings are secondary consequences of the observed muscle fiber abnormalities due to lack of DNM2. Along these lines, we also found massive accumulations of highly ubiquitinated proteins and an upregulation of the lysosomal marker LAMP1 in DNM2 null muscles (Supplementary Material, Fig. S3), consistent with an impairment of degradative properties of the proteasomal/lysosomal pathways. Taken together, these results indicate an intriguing and obligatory link between DNM2 function and various lipid-regulated events in skeletal muscle.

DNM2 in skeletal muscle is required for proper mitochondrial morphology and function

LDs interact with mitochondria and offer them the substrate for β-oxidation to generate energy (18). Thus, we examined mitochondria in mouse skeletal muscles lacking DNM2. Morphologically, mitochondrial shapes (Fig. 7A and B) and sizes (Fig. 8D) appeared to be normal in gastrocnemius muscles of *HSACreDnm2*$^{fl/fl}$ mice compared with controls at P5. However, the density of mitochondria was reduced in mutants (Fig. 8A). In P10 mutants, we found a similar reduction (Fig. 8B), but in striking contrast to the findings at P5, there was also a remarkable disruption of the mitochondrial morphology, particularly affecting mitochondrial cristae (Fig. 7C and D). In addition, the size of mitochondria was altered with a marked shift toward larger mitochondria in mutants (Fig. 8E). To examine whether the observed morphological variations correspond to alterations in the respiratory chain of mitochondria, we analyzed protein expression levels of the 39 kDa subunit of the respiratory complex I (CI) and of the 70 kDa subunit of the respiratory complex II (CII), both located in the inner mitochondrial membrane in gastrocnemius muscles. Additionally, we measured VDAC1 (porin) protein expression as a marker of the outer mitochondrial membrane. CI and CII were decreased at P5 and P10 in *HSACreDnm2*$^{fl/fl}$ mice compared with controls, while VDAC1 was unaltered (Fig. 8C). In summary, these results demonstrate that DNM2 is required in skeletal muscle to assure correct mitochondria numbers, structure and function.

DNM2 in skeletal muscle is required for proper neuromuscular junctions and peripheral nerve stability

In some pathological conditions (20,21), alterations of muscle-resident mitochondria correlate with the aberrant structure and function of the neuromuscular junction (NMJ). Furthermore,

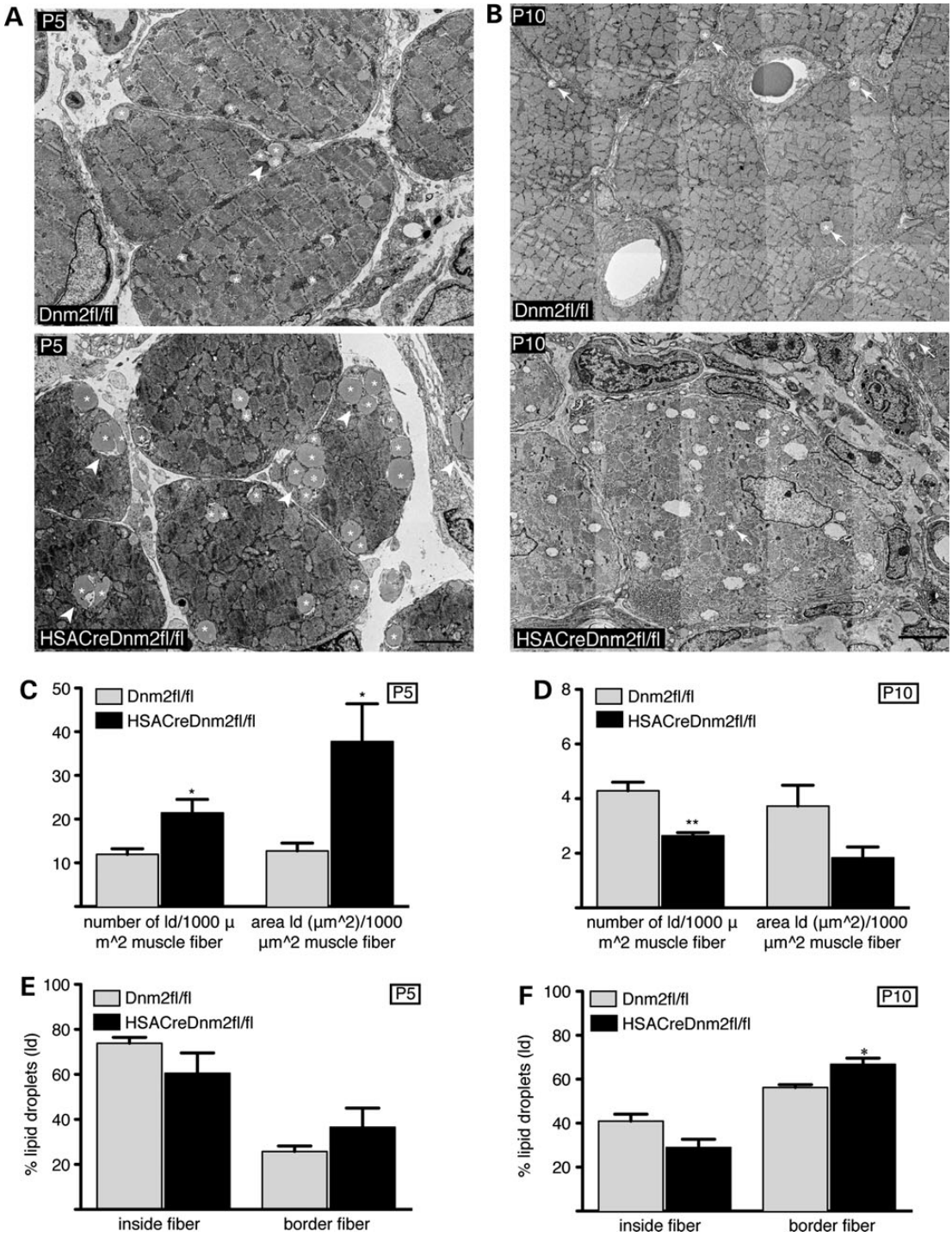

Figure 4. Lack of DNM2 causes dysregulation of LDs in skeletal muscle (electron microscopy analysis). Ultrathin sections of gastrocnemius muscles of HSA-CreDnm2$^{fl/fl}$ mutant mice and Dnm2$^{fl/fl}$ controls at P5 (**A**) and P10 (**B**) analyzed by electron microscopy. Exemplary LDs are marked by asterisks in (A) and with an additional arrow in (B). Cluster formation of LDs is highlighted by arrowheads. Scale bars = 5 µM. (**C** and **D**) Quantitative analysis of the number of LDs per muscle area and of the ratios between the area occupied by LDs and the muscle area is depicted for mutants and controls at P5 and P10. (**E** and **F**) Analyses of ld localizations are shown in mutant and control muscles at P5 and P10. LD localizations have been distinguished as inside fiber (localized in the core of the fibers) or border fiber (touching the sarcolemma). Three animals were analyzed for each genotype and developmental age; $^{*}P < 0.05$, $^{**}P < 0.01$.

proper protein transport and clustering of acetylcholine receptors (AChRs) in the sarcolemma are crucial for correctly structured NMJs. Given the mitochondrial deficiencies in *HSA-CreDnm2$^{fl/fl}$* mice and the known pleiotropic functions of DNM2 in the regulation of endosomes and the cytoskeleton, we asked whether NMJs require DNM2 in skeletal muscle. Since the diaphragm was also affected, we examined this issue by preparing whole mount diaphragm muscles from P5 *HSACreDnm2$^{fl/fl}$*

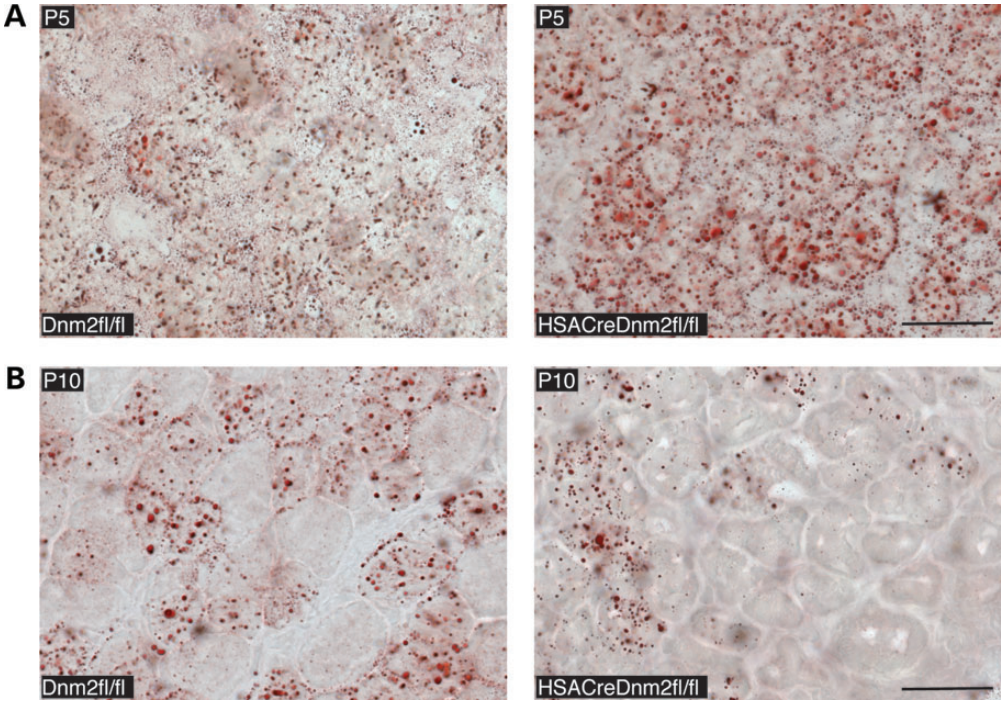

Figure 5. Effects of DNM2 ablation on LDs in skeletal muscle (histological analysis). Oil red O staining for LDs of (**A**) P5 and (**B**) P10 sections of gastrocnemius muscles of HSACreDnm2$^{fl/fl}$ mutant and control mice. Three animals have been analyzed and representative pictures are shown. Scale bar = 30 μM.

mice and controls. AChRs were identified using incubation with labeled alpha-bungarotoxin and axons were labeled with antibody-based neurofilament staining. Analysis by confocal microscopy revealed increased sizes of neuromuscular endplates in mutant mice compared with controls, with diffusely organized AChR in mutants (Fig. 9A and B). We conclude that lack of DNM2 in muscles alters NMJs and may affect normal clustering of AChRs.

Next, we hypothesized that the observed muscle and NMJ alterations may also affect nerve integrity. Thus, we analyzed the morphology of intramuscular nerves of *HSACreDnm2*$^{fl/fl}$ mice and controls at P10. Remak bundles appeared in a regular shape and axons were normally myelinated in mutant mice, but there were frequent signs of axonal degeneration (Fig. 9C and D; 4.68 ± 0.16% axons affected in mutants versus 0.86 ± 0.02% in controls; $n = 3$ mice; at least 2000 axons counted in each condition). Thus, the dependence of skeletal muscles on DNM2 is propagated to cause axonal degeneration in peripheral nerves, rendering them indirectly dependent on skeletal-muscle expressed DNM2. Mitochondria dysfunction in the muscle and defective NMJ are likely to contribute to this chain of deleterious events.

DISCUSSION

Two disorders are associated with mutations in the gene encoding the large GTPase DNM2. Primarily peripheral nerves are affected in DI-CMT, while skeletal muscles are primarily affected in CNM. Both diseases are dominantly inherited. Studies aimed at determining the underlying disease mechanisms in various transgenic mice and cell culture models revealed predominantly gain-of-functions and/or dominant-negative effects of mutant DNM2 proteins. However, partial loss-of-function has also been suggested for a particular DNM2 mutant with a very severe phenotype in the homozygous state (22). To elucidate this issue further and to determine the necessity of DNM2 in normal physiology, we used gene targeting in the mouse. An ubiquitous loss of DNM2 turned out to be embryonically lethal at an early developmental stage [our unpublished data (23)]. This finding precluded further analyses of muscles, our intended primary focus in this study based on the key role of this tissue in DNM2-CNM. Thus, we resorted to a conditional *Dnm2*$^{fl/fl}$ allele (2), in combination with cell type-specific Cre recombinase expression, to eliminate DNM2 specifically from skeletal muscle cells *in vivo*. We found that DNM2 expression in skeletal muscles is an obligatory prerequisite for accurate mouse development. Specific analyses revealed that DNM2 function is required for correct muscle fiber numbers, sizes and survival. Mitochondria and proper regulation of lipid metabolism, in particular the dynamics of LDs, are dependent on DNM2. Furthermore, we found that muscle-specific loss of DNM2 caused enlargements of neuromuscular endplates accompanied by axonal damage in intramuscular nerves.

As expected from the analysis of heterozygous *Dnm2* null mice, we did not detect a phenotype in mice carrying a muscle-specific heterozygous *Dnm2* deletion (data not shown). This finding allowed us to focus our analyses on mice lacking DNM2 in muscle cells. As most obvious features, these animals had decreased muscle mass, loss of muscle fibers and severe alterations in muscle morphology early in postnatal life. Our examinations indicate that the observed myopathy is likely due to loss of muscle fibers, in combination with atrophic fibers, rather than a delay in fiber maturation. The defects caused general weakness and death of the animals around P14.

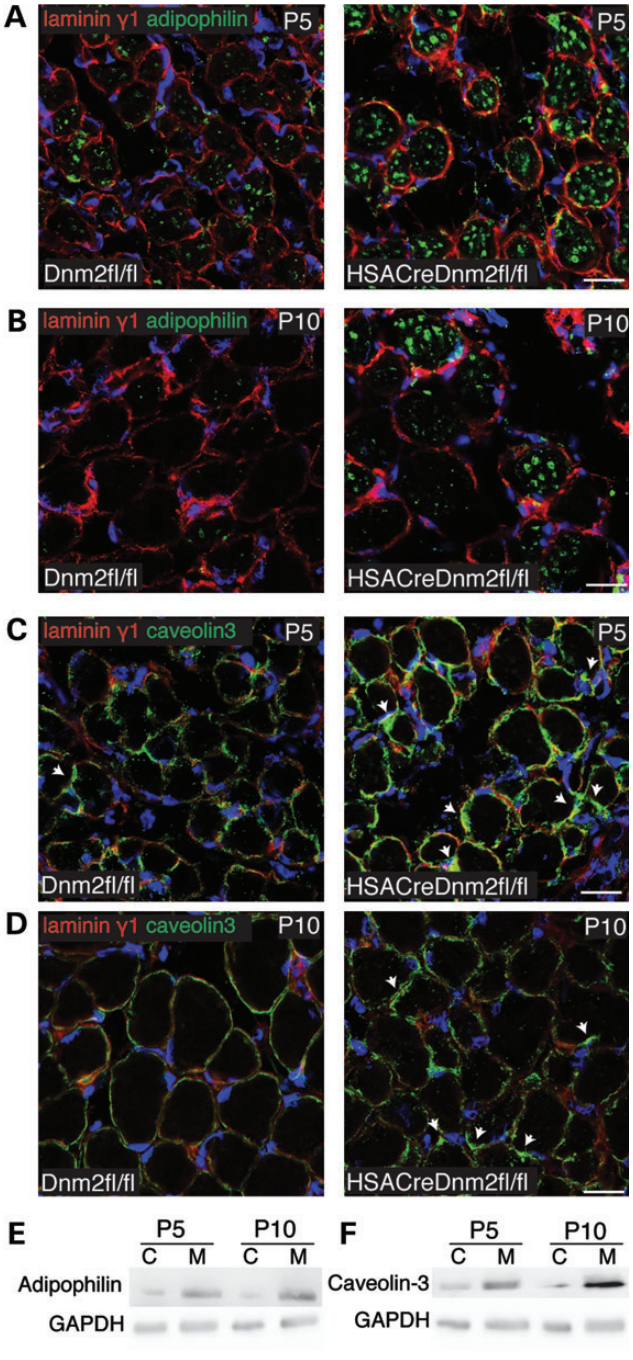

Figure 6. DNM2 ablation in muscle cells causes increased expression and altered localization of the LD-associated protein adipophilin and caveolin 3. Cross-sections of gastrocnemius muscles of HSACreDnm2$^{fl/fl}$ mutant mice and Dnm2$^{fl/fl}$ controls at P5 (**A** and **C**) and P10 (**B** and **D**) stained with antibodies recognizing laminin γ1 (red) and adipophilin (green; A and B) or caveolin 3 (green; C and D). Arrows in (C) and (D) indicate areas with accumulation of caveolin 3. Western blot analyses of gastrocnemius protein lysates from mutants and controls at P5 and P10 show increased expression levels of adipophilin (**E**) and caveolin 3 (**F**) in mutants (marked M) compared with controls (marked C). Pictures and western blots are representative of three independent experiments. Scale bar = 15 μM.

Consequently, we restricted our analyses to time points up to P10 on animal welfare grounds. Analyses of long-term effects of loss of DNM2 in muscle will require the development of suitable hypomorphic *Dnm2* alleles, or targeting the loss of DNM2 to specific muscle groups using appropriate germline transgenic methods or viral vector-based approaches.

Ablation of DNM2 in skeletal muscle cells caused a strong increase in LDs in muscles at P5. LDs contain neutral lipids and regulate their storage and hydrolysis. In doing so, LDs store metabolic energy and membrane components (17). Furthermore, LDs are motile and appear to interact with the endoplasmic reticulum, endosomes, peroxisomes and mitochondria in distributing lipids to those organelles (24). These processes include vesiculation in response to metabolic demands and can depend on the vesicle scission activity of the dynamin mechanoenzyme (Susan Chi and Marc McNiven, personal communication). It appears to be plausible that disturbances of these physiologically important activities contribute to our observation of increased LDs in DNM2-deficient muscle cells. Since the levels of fatty acid synthase (FASN), the key enzyme involved in the synthesis of fatty acids, are not altered in DNM2-deficient muscles at P5 or P10 (Supplementary Material, Fig. S3C), increased cell-autonomous lipogenesis is unlikely to be a major contributor to the increased LDs. However, LD build-up due to altered cell metabolism remains to be considered since LD accumulation in muscles can be induced through treatment with toxic substances [Fialuridine (25), Zidovudina (26)] and is found in pathological states such as diabetes, atherosclerosis and metabolic disorders (27,28). Whether and to which degree these pathological states are interconnected with the regulation of DNM-mediated LD dynamics remains a challenging question for the future.

One suggested function of LDs is providing lipids to mitochondria for ß-oxidation (29). Generally, LDs and mitochondria are found in close apposition inside the cells. Furthermore, the SNARE family protein SNAP23 plays an important role in LD fusion (30,31) and in generating LD-mitochondrial complexes, affecting ß-oxidation and possibly involving fusion of LDs with mitochondria (32). Indeed, such a close association/fusion may explain our surprising observation of numerous structures that were positive for the LD marker adipophilin in DNM2-deficient muscles at P10, when LDs were not increased anymore compared with control muscles. In the context of the close structural and functional association between LDs and mitochondria, it is remarkable that ablation of DNM2 in skeletal muscle cells in our study was correlated with massive mitochondria enlargements and disruptions of cristae at P10. In addition, expression of subunits of the respiratory complexes I and II was reduced already at P5, indicating early negative physiological consequences of DNM2 loss on mitochondria.

Swollen mitochondria harboring disorganized cristae have also been observed in a mouse model of diabetes, and LD accumulation and mitochondrial dysfunction are typically detected in insulin resistance type 2 diabetic mice (20,33,34). Insulin resistance is a hallmark of type 2 diabetes and is also found in patients affected by insulin-resistant syndrome or dysmetabolic syndrome (35). Cell culture experiments have shown that expression of DNM-K44A results in specific alterations of the insulin receptor signaling pathway by inhibiting clathrin-mediated endocytosis of the insulin receptor in adipocyte, resulting in an increased basal rate of glucose uptake, glycogen synthesis and lipogenesis (36). Comparing these findings and the consequences of insulin resistance with our data in DNM2-

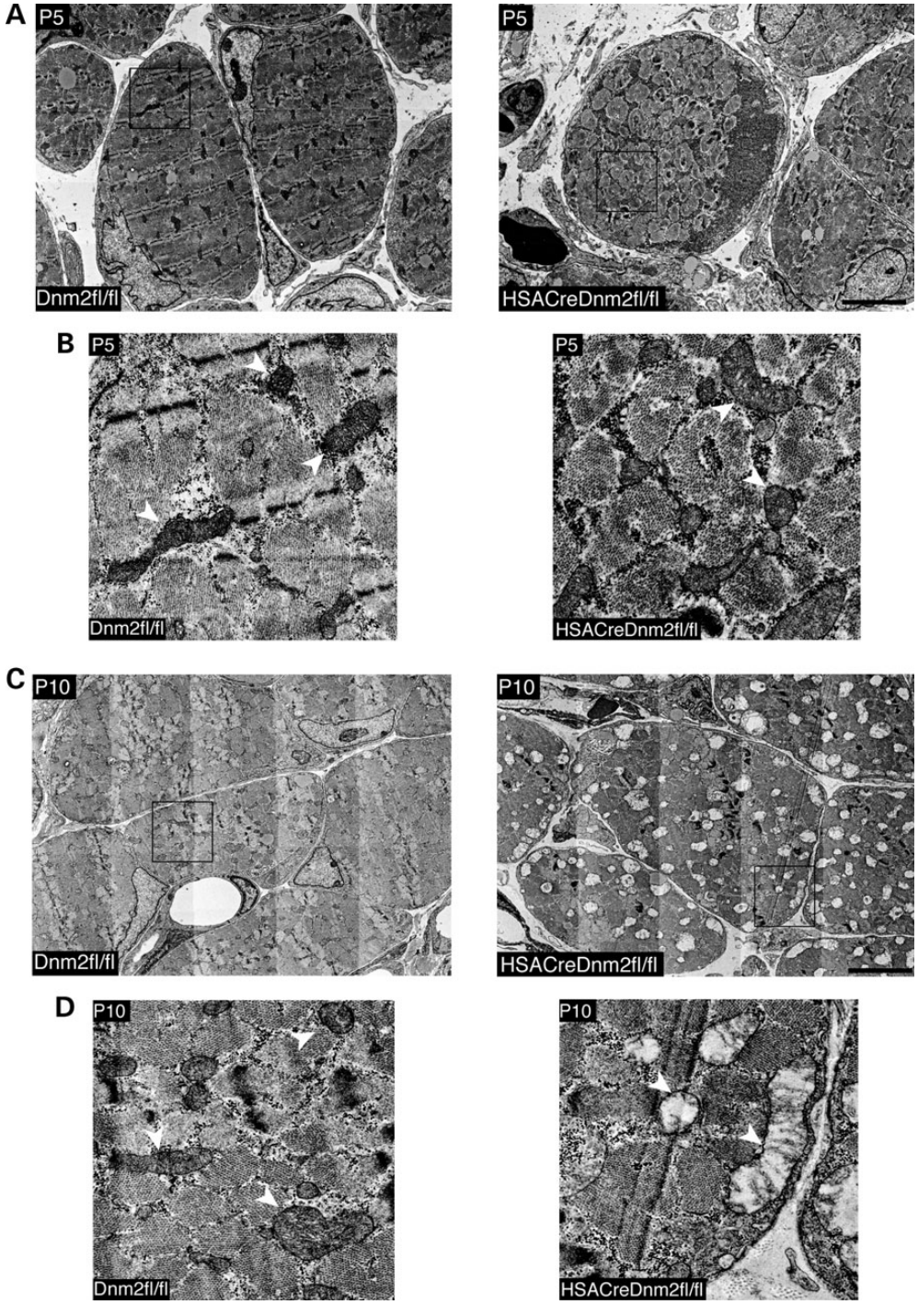

Figure 7. DNM2 deficiency induces morphological mitochondrial aberrations. Electron microscopy-derived pictures of ultrathin sections of gastrocnemius muscles of HSACreDnm2$^{fl/fl}$ mutant mice and Dnm2$^{fl/fl}$ controls at P5 (**A**) and P10 (**C**) are shown. Scale bars = 5 μM. Square areas in (A) and (C) are enlarged in (**B**) and (**D**), respectively, to highlight the swollen mitochondrial structure and disruption of cristae at P10. Arrowheads indicate mitochondria (B and D).

deficient muscles reveals interesting parallels and warrants further investigations.

Altered NMJs are an additional feature in murine models of diabetes (36) and recent data implicate NMJ abnormalities also in DNM2-CNM (37). We found increased sizes of neuromuscular endplates in muscle-specific DNM2-deficient mice. Thus, loss of DNM2 function in muscle is sufficient to severely alter the morphology of NMJs, most likely affecting also their physiology and contributing to the macroscopic phenotype of the mice. This requirement of muscle-expressed DNM2 must be taken into account if interpreting NMJ deficits in disease. Given the multiple defects observed in muscles lacking

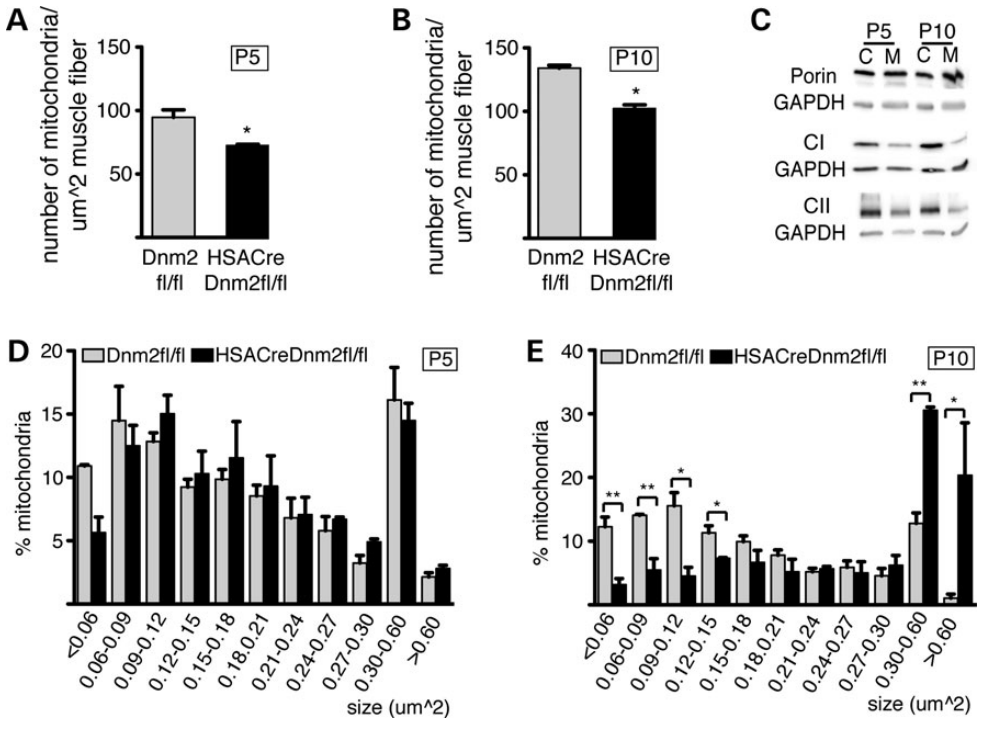

Figure 8. Quantification of DNM2 deficiency-induced mitochondrial aberrations. Quantification of the density of mitochondria reveals a reduction in mutants compared with controls at P5 (**A**) and P10 (**B**). While mitochondrial size distribution is not altered in mutants at P5 (**D**), there is a strong shift toward larger mitochondria in the mutants versus controls at P10 (**E**). Three animals have been analyzed for each genotype and developmental age. (**C**) Western blot analysis of selected mitochondrial proteins in gastrocnemius protein lysates of HSACreDnm2$^{fl/fl}$ mutant mice and Dnm2$^{fl/fl}$ controls at P5 and P10. Porin (VDAC1) was used as a marker of the outer membrane. The 39 kDa subunit of the NADH ubiquinone oxidoreductase of respiratory CI and the 70 kDa subunit of the respiratory CII were employed as markers of the inner mitochondrial membrane. GAPDH served as loading control. Representative western blots out of four independent experiments are shown; $^{*}P < 0.05$, $^{**}P < 0.01$.

DNM2, however, the direct course of events leading to NMJ alterations remains largely speculative. Flawed mitochondrial function may be involved (36). Another likely contribution might come from altered AChR clustering. Lack of DNM2 could interfere with trafficking of proteins important for clustering and/or affect the biosynthesis and signaling of the AChR receptor (38). A potential regulatory role of LDs must also be considered since LDs can serve as regulators of membrane biogenesis and may affect signaling.

An intriguing finding in our study was the damage of peripheral nerves, secondary to restricted DNM2 deficiency in muscles. It is well known that development and maintenance of NMJs is a dynamic process that involves both muscles and nerves depending on each other. Muscle abnormalities in energy metabolism can cause denervation (21) and thus, nerve damage in specifically DNM2-deficient muscles might be due to the observed mitochondrial alterations. However, altered protein biosynthesis, metabolism and/or trafficking that affect the NMJ may contribute by affecting proper signaling from muscle to axon and provoking axonal instability and degeneration.

Taken together, we demonstrate that DNM2 function in muscle cells is an absolute requirement for muscles and, indirectly, peripheral nerve biology. In addition to the well-known molecular functions of DNM2 as worked out in cell culture and by biochemical approaches, we propose that lipid and energy metabolism are key physiological processes that are regulated and dependent on the proper function of this central large GTPase. Our findings warrant particularly future investigations in the functional roles of DNM2 in LD dynamics and its associated regulatory processes. We anticipate that such studies will provide important knowledge relevant to develop new approaches to tackle not only CNM but also insulin resistance-like syndromes.

MATERIALS AND METHODS

Mice

Experiments followed approved protocols (Veterinary Office, Canton Zurich, Switzerland). Mice carrying LoxP flanking exon 2 of the DNM2 gene (2) were breed with mice carrying a transgene encoding Cre recombinase under the control of human skeletal actin (HSA) regulatory elements [(16); kind gift of Dr Ulrich Müller, Scripps Research Institute, La Jolla, USA]. Genotypes of mice were determined by polymerase chain reaction on genomic DNA.

Electron microscopy

Anesthesia of mice was achieved with an IP injection of 150 mg/kg pentobarbital (Nembutal; Abbott Laboratories). Mice were perfused with 1% heparin sodium in 0.1 M phosphate buffer (pH 7.4), followed by 3% glutardialdehyde and 4% paraformaldehyde (PFA) in 0.1 M phosphate buffer. Fixed muscle tissues were post-fixed in 2% osmium tetroxide, dehydrated via a

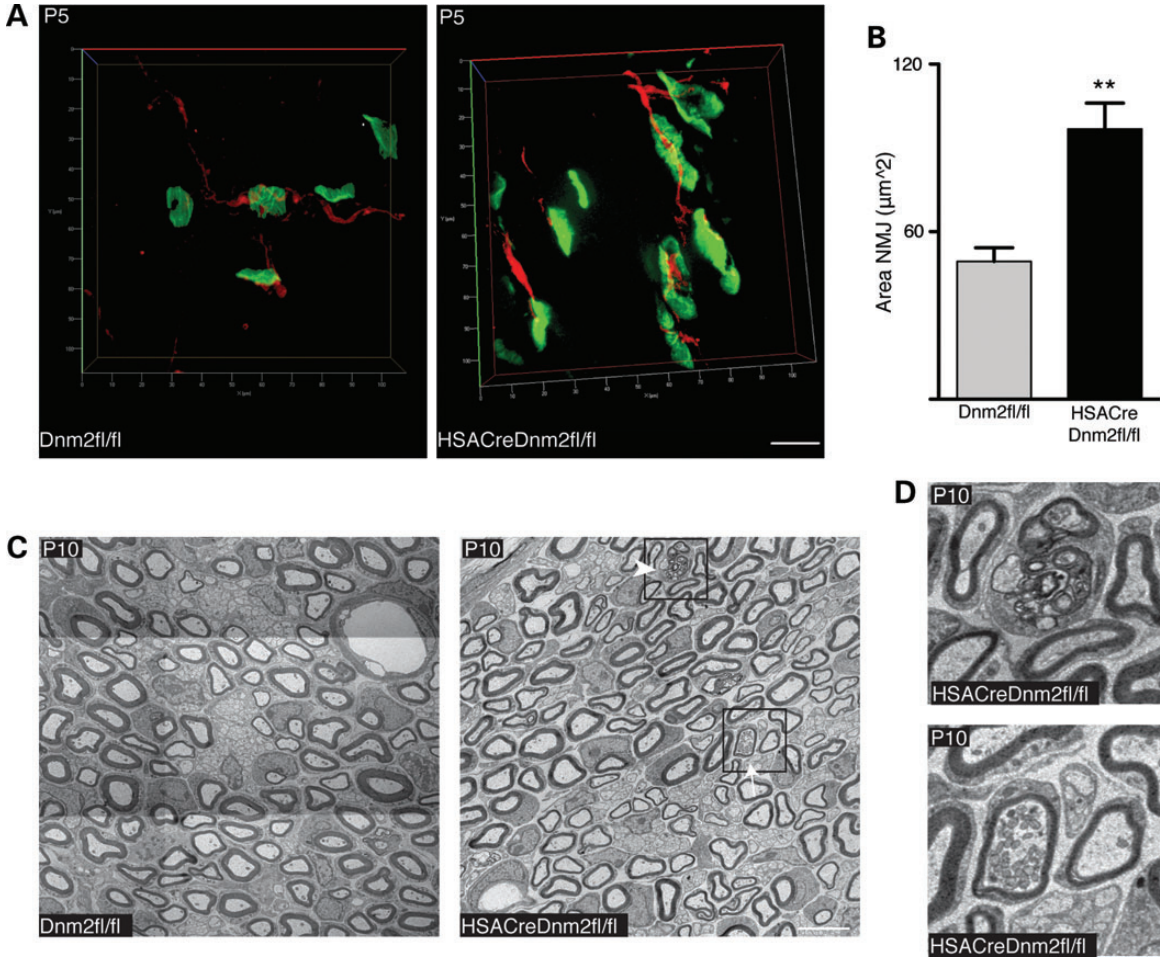

Figure 9. Ablation of DNM2 in muscle leads to altered NMJs and axonal degeneration. 3D confocal reconstructions (**A**) of NMJ staining of whole mount diaphragm muscles are shown. Neurofilament (red), bungarotoxin (green). (**B**) Quantification of the area occupied by AChR based on Z-stack confocal images of entire NMJ. Three animals have been analyzed for each genotype with at least 20 NMJs measured per animal. (**C** and **D**) Electron microscopy-derived pictures of intramuscular nerves show degenerated (arrowheads) and degenerating (arrow) axons in HSACreDnm2fl/fl mutants. $^{**}P < 0.01$ (B and C) Scale bar = 10 µM.

graded acetone series and embedded in Spurr's resin (EMS as described previously (39). Ultrathin sections were contrasted with 3% uranyl acetate and 1% lead citrate before analysis in a transmission electron microscope (FEI Morgagni 268, FEI Electron Optics, The Netherlands).

Histochemical stainings

After dissection, muscles were frozen by immersion in liquid nitrogen-cooled isopentan. Ten micrometer muscle sections were cut on a cryostat and hematoxylin/eosin staining was carried out as described (40). Masson's trichrome staining (41) was performed using a commercial kit (HT-15; Trichrome Stain Kit; Sigma-Aldrich).

LDs and mitochondria

The size of LDs and mitochondria was evaluated using CS5 Photoshop analysis software.

Immunohistochemistry analysis

P5 and P10 gastrocnemius muscles were dissected from mice of different genotypes and frozen through immersion in liquid nitrogen-cooled isopentane. Ten micrometer sections were obtained using a cryostat. The sections were permeabilized and fixed according to the detecting antibody used. For dMHC stainings, the sections were fixed for 10 min with 4% PFA, washed three times in phosphate-buffered saline (PBS) and blocked 1 h at room temperature in 20% goat serum, 2% bovine serum albumin (BSA), 0.1% Triton in PBS. Sections were then incubated with dMHC (Leica) and rat anti laminin γ1 (Millipore) over night at 4°C. After three washes in PBS, the sections were incubated with Cy3-conjugated anti-rabbit (Jackson Laboratories, 1:500) and Alexa488-conjugated anti-rat (Molecular Probes, 1:500) antibodies in blocking buffer for 1 h at room temperature, and washed with PBS. After 5 min incubation with DAPI solution, the sections were washed and mounted with IMMU-MOUNT (Thermo Fisher Scientific, Germany). Adipophilin and caveolin 3 stainings were performed as described (26). Antibodies used were rabbit anti-adipophilin

(Abcam) and rabbit anti-caveolin 3 (Enzo Life Science). Images were generated with a confocal inverted microscope (Leica SP2-AOBS) using argon and helium/neon lasers and imported to Adobe Photoshop CS5 for level adjustment, cropping and merging. To analyze NMJs, whole mount diaphragm muscles were dissected and freshly fixed in 4% PFA. After 30 min incubation with bungarotoxin-FITC (Molecular Probes), the tissue was treated for 2 h with blocking buffer (PBT: 1% Triton X-100, 2% BSA in PBS). Samples were incubated overnight with a primary mouse antibody against neurofilament (Chemicon). After 10 washes in PBT, specimens were incubated for 3 h with secondary antibody anti mouse-CY3 antibodies in PBT at 4°C. Then preparations were washed three times for 30 min in PBT, once for 5 min in PBS and post-fixed for 10 min in 1% PFA. Finally, samples were mounted and analyzed by confocal microscopy.

Oil red O

Three parts of Oil red O stock solution (0.5% Oil red O in isopropanol) were diluted with two parts of H_2O. Muscle sections, fixed for 1 h at room temperature using 3.7% formaldehyde solution, were rinsed three times for 30 s in H_2O, immersed in the Oil red O working solution for 30 min, rinsed with H_2O for 10 min and mounted with IMMU-MOUNT (Thermo Fisher Scientific) (42).

Western blot analysis

Gastrocnemius muscles were dissected and frozen in liquid nitrogen. Muscle samples were placed in a dry ice pre-cooled metal pestle and homogenized. The generated powder was collected and re-suspended in 250 µl lysis buffer (95 mM NaCl, 25 mM Tris–Cl pH 7.4, 10 mM EDTA, 2% SDS, 1:100 protease inhibitor, 1:100 NaF, 1: 100 Na_2V_3). Samples were sonicated twice for 5 min, with vortexing in between, boiled for 5 min and centrifuged for 5 min. Supernatants were collected and protein quantification was performed with the Pierce® BCA Protein Assay kit (Thermo scientific). Fifteen micrograms of protein lysates were then analyzed by standard blotting techniques. Signals were quantified using Fusion Fx7 Image J software. Antibodies used: rabbit anti-Dnm1 (Abcam), rabbit anti-Dnm2 (2), rabbit anti-Dnm3 (Abcam), rabbit anti-dMHC (Leica), rabbit anti-MHC (Cell Signaling), rabbit anti-adipophilin (Abcam), rabbit anti-caveolin 3 (Enzo Life Science), mouse anti-ubiquitin (Santa Cruz), rat anti-LAMP1 (DSHB), rabbit anti-FASN (Abcam), mouse anti-VDAC1 (Abcam), mouse anti-subunit 39 kDa Complex1 (Molecular Probes) and mouse anti-subunit 70 kDa Complex 2 (Molecular Probes).

Statistical analysis

Data represent the average and the standard error of the mean of at least three independent experiments if not indicated differently. Statistical analysis was performed via a two-tailed Student's *t*-test.

SUPPLEMENTARY MATERIAL

Supplementary Material is available at *HMG* online

ACKNOWLEDGEMENTS

We thank Dr Markus Rüegg and Dr Shuo Lin (both University of Basel) and the members of the Suter laboratory for valuable advice and fruitful discussions. We are also grateful to the Electron Microscopy Center and the Light Microscopy Center of the ETH Zurich for support.

Conflict of Interest statement. None declared.

FUNDING

This work was supported by the Swiss National Science Foundation and the National Centre of Competence in Research (NCCR), Neural Plasticity and Repair.

REFERENCES

1. Durieux, A.C., Vignaud, A., Prudhon, B., Viou, M.T., Beuvin, M., Vassilopoulos, S., Fraysse, B., Ferry, A., Laine, J., Romero, N.B. *et al.* (2010) A centronuclear myopathy-dynamin 2 mutation impairs skeletal muscle structure and function in mice. *Hum. Mol. Genet.*, **19**, 4820–4836.
2. Sidiropoulos, P.N., Miehe, M., Bock, T., Tinelli, E., Oertli, C.I., Kuner, R., Meijer, D., Wollscheid, B., Niemann, A. and Suter, U. (2012) Dynamin 2 mutations in Charcot-Marie-Tooth neuropathy highlight the importance of clathrin-mediated endocytosis in myelination. *Brain*, **135**, 1395–1411.
3. Jungbluth, H., Wallgren-Pettersson, C. and Laporte, J. (2008) Centronuclear (myotubular) myopathy. *Orphanet J. Rare Dis.*, **3**, 26.
4. Romero, N.B. (2010) Centronuclear myopathies: a widening concept. *Neuromuscul. Disord.*, **20**, 223–228.
5. Durieux, A.C., Vassilopoulos, S., Laine, J., Fraysse, B., Brinas, L., Prudhon, B., Castells, J., Freyssenet, D., Bonne, G., Guicheney, P. *et al.* (2012) A centronuclear myopathy—dynamin 2 mutation impairs autophagy in mice. *Traffic*, **13**, 869–879.
6. Cowling, B.S., Toussaint, A., Muller, J. and Laporte, J. (2012) Defective membrane remodeling in neuromuscular diseases: insights from animal models. *PLoS Genet.*, **8**, e1002595.
7. Ferguson, S.M. and De Camilli, P. (2012) Dynamin, a membrane-remodelling GTPase. *Nat. Rev. Mol. Cell. Biol.*, **13**, 75–88.
8. Schmid, S.L. and Frolov, V.A. (2011) Dynamin: functional design of a membrane fission catalyst. *Annu. Rev. Cell. Dev. Biol.*, **27**, 79–105.
9. Kenniston, J.A. and Lemmon, M.A. (2010) Dynamin GTPase regulation is altered by PH domain mutations found in centronuclear myopathy patients. *EMBO J.*, **29**, 3054–3067.
10. Wang, L., Barylko, B., Byers, C., Ross, J.A., Jameson, D.M. and Albanesi, J.P. (2010) Dynamin 2 mutants linked to centronuclear myopathies form abnormally stable polymers. *J. Biol. Chem.*, **285**, 22753–22757.
11. Zuchner, S., Noureddine, M., Kennerson, M., Verhoeven, K., Claeys, K., De Jonghe, P., Merory, J., Oliveira, S.A., Speer, M.C., Stenger, J.E. *et al.* (2005) Mutations in the pleckstrin homology domain of dynamin 2 cause dominant intermediate Charcot-Marie-Tooth disease. *Nat. Genet.*, **37**, 289–294.
12. Cowling, B.S., Toussaint, A., Amoasii, L., Koebel, P., Ferry, A., Davignon, L., Nishino, I., Mandel, J.L. and Laporte, J. (2011) Increased expression of wild-type or a centronuclear myopathy mutant of dynamin 2 in skeletal muscle of adult mice leads to structural defects and muscle weakness. *Am. J. Pathol.*, **178**, 2224–2235.
13. Liu, N., Bezprozvannaya, S., Shelton, J.M., Frisard, M.I., Hulver, M.W., McMillan, R.P., Wu, Y., Voelker, K.A., Grange, R.W., Richardson, J.A. *et al.* (2011) Mice lacking microRNA 133a develop dynamin 2-dependent centronuclear myopathy. *J. Clin. Invest.*, **121**, 3258–3268.
14. Gibbs, E.M., Davidson, A.E., Trickey-Glassman, A., Backus, C., Hong, Y., Sakowski, S.A., Dowling, J.J. and Feldman, E.L. (2013) Two dynamin-2 genes are required for normal zebrafish development. *PLoS ONE*, **8**, e55888.
15. Leu, M., Bellmunt, E., Schwander, M., Farinas, I., Brenner, H.R. and Muller, U. (2003) Erbb2 regulates neuromuscular synapse formation and is essential for muscle spindle development. *Development*, **130**, 2291–2301.
16. Agbulut, O., Noirez, P., Beaumont, F. and Butler-Browne, G. (2003) Myosin heavy chain isoforms in postnatal muscle development of mice. *Biol. Cell*, **95**, 399–406.

17. Walther, T.C. and Farese, R.V. Jr (2012) Lipid droplets and cellular lipid metabolism. *Annu. Rev. Biochem.*, **81**, 687–714.
18. McManaman, J.L., Zabaronick, W., Schaack, J. and Orlicky, D.J. (2003) Lipid droplet targeting domains of adipophilin. *J. Lipid Res.*, **44**, 668–673.
19. Gazzerro, E., Sotgia, F., Bruno, C., Lisanti, M.P. and Minetti, C. (2009) Caveolinopathies: from the biology of caveolin-3 to human diseases. *Eur. J. Hum. Genet.*, **18**, 137–145.
20. Fahim, M.A., Hasan, M.Y. and Alshuaib, W.B. (2000) Early morphological remodeling of neuromuscular junction in a murine model of diabetes. *J. Appl. Physiol.*, **89**, 2235–2240.
21. Dupuis, L., Gonzalez de Aguilar, J.L., Echaniz-Laguna, A., Eschbach, J., Rene, F., Oudart, H., Halter, B., Huze, C., Schaeffer, L., Bouillaud, F. *et al.* (2009) Muscle mitochondrial uncoupling dismantles neuromuscular junction and triggers distal degeneration of motor neurons. *PLoS ONE*, **4**, e5390.
22. Koutsopoulos, O.S., Kretz, C., Weller, C.M., Roux, A., Mojzisova, H., Bohm, J., Koch, C., Toussaint, A., Heckel, E., Stemkens, D. *et al.* (2012) Dynamin 2 homozygous mutation in humans with a lethal congenital syndrome. *Eur. J. Hum. Genet.*, **21**, 637–642.
23. Ferguson, S.M., Raimondi, A., Paradise, S., Shen, H., Mesaki, K., Ferguson, A., Destaing, O., Ko, G., Takasaki, J., Cremona, O. *et al.* (2009) Coordinated actions of actin and BAR proteins upstream of dynamin at endocytic clathrin-coated pits. *Dev. Cell*, **17**, 811–822.
24. Zehmer, J.K., Huang, Y., Peng, G., Pu, J., Anderson, R.G. and Liu, P. (2009) A role for lipid droplets in inter-membrane lipid traffic. *Proteomics*, **9**, 914–921.
25. Lewis, W., Griniuviene, B., Tankersley, K.O., Levine, E.S., Montione, R., Engelman, L., de Courten-Myers, G., Ascenzi, M.A., Hornbuckle, W.E., Gerin, J.L. *et al.* (1997) Depletion of mitochondrial DNA, destruction of mitochondria, and accumulation of lipid droplets result from fialuridine treatment in woodchucks (Marmota monax). *Lab. Invest.*, **76**, 77–87.
26. Dalakas, M.C., Leon-Monzon, M.E., Bernardini, I., Gahl, W.A. and Jay, C.A. (1994) Zidovudine-induced mitochondrial myopathy is associated with muscle carnitine deficiency and lipid storage. *Ann. Neurol.*, **35**, 482–487.
27. Greenberg, A.S., Coleman, R.A., Kraemer, F.B., McManaman, J.L., Obin, M.S., Puri, V., Yan, Q.W., Miyoshi, H. and Mashek, D.G. (2011) The role of lipid droplets in metabolic disease in rodents and humans. *J. Clin. Invest.*, **121**, 2102–2110.
28. Lusis, A.J., Attie, A.D. and Reue, K. (2008) Metabolic syndrome: from epidemiology to systems biology. *Nat. Rev. Genet.*, **9**, 819–830.
29. Reue, K. (2011) A thematic review series: lipid droplet storage and metabolism: from yeast to man. *J Lipid Res.*, **52**, 1865–1868.
30. Bostrom, P., Rutberg, M., Ericsson, J., Holmdahl, P., Andersson, L., Frohman, M.A., Boren, J. and Olofsson, S.O. (2005) Cytosolic lipid droplets increase in size by microtubule-dependent complex formation. *Arterioscler. Thromb. Vasc. Biol.*, **25**, 1945–1951.
31. Bostrom, P., Andersson, L., Rutberg, M., Perman, J., Lidberg, U., Johansson, B.R., Fernandez-Rodriguez, J., Ericson, J., Nilsson, T., Boren, J. *et al.* (2007) SNARE Proteins mediate fusion between cytosolic lipid droplets and are implicated in insulin sensitivity. *Nat. Cell Biol.*, **9**, 1286–1293.
32. Jagerstrom, S., Polesie, S., Wickstrom, Y., Johansson, B.R., Schroder, H.D., Hojlund, K. and Bostrom, P. (2009) Lipid droplets interact with mitochondria using SNAP23. *Cell Biol. Int.*, **33**, 934–940.
33. Abdul-Ghani, M.A. and DeFronzo, R.A. (2008) Mitochondrial dysfunction, insulin resistance, and type 2 diabetes mellitus. *Curr. Diab. Rep.*, **8**, 173–178.
34. Machann, J., Haring, H., Schick, F. and Stumvoll, M. (2004) Intramyocellular lipids and insulin resistance. *Diabetes Obes. Metab.*, **6**, 239–248.
35. Abdul-Ghani, M.A., Matsuda, M. and DeFronzo, R.A. (2008) Strong association between insulin resistance in liver and skeletal muscle in non-diabetic subjects. *Diabet. Med.*, **25**, 1289–1294.
36. Ceresa, B.P., Kao, A.W., Santeler, S.R. and Pessin, J.E. (1998) Inhibition of clathrin-mediated endocytosis selectively attenuates specific insulin receptor signal transduction pathways. *Mol. Cell. Biol.*, **18**, 3862–3870.
37. Gibbs, E.M., Clarke, N.F., Rose, K., Oates, E.C., Webster, R., Feldman, E.L. and Dowling, J.J. (2013) Neuromuscular junction abnormalities in DNM2-related centronuclear myopathy. *J. Mol. Med. (Berl)*, **91**, 727–737.
38. Punga, A.R. and Ruegg, M.A. (2012) Signaling and aging at the neuromuscular synapse: lessons learnt from neuromuscular diseases. *Curr. Opin. Pharmacol.*, **12**, 340–346.
39. Pereira, J.A., Baumann, R., Norrmen, C., Somandin, C., Miehe, M., Jacob, C., Luhmann, T., Hall-Bozic, H., Mantei, N., Meijer, D. *et al.* (2010) Dicer in Schwann cells is required for myelination and axonal integrity. *J. Neurosci.*, **30**, 6763–6775.
40. Wrabetz, L., Feltri, M.L., Quattrini, A., Imperiale, D., Previtali, S., D'Antonio, M., Martini, R., Yin, X., Trapp, B.D., Zhou, L. *et al.* (2000) P(0) glycoprotein overexpression causes congenital hypomyelination of peripheral nerves. *J. Cell Biol.*, **148**, 1021–1034.
41. Luna, L.G. (1968) *Manual of Histologic Staining Methods of the Armed Forces Institute of Pathology*. McGraw-Hill, New York.
42. Koopman, R., Schaart, G. and Hesselink, M.K. (2001) Optimisation of oil red O staining permits combination with immunofluorescence and automated quantification of lipids. *Histochem. Cell Biol.*, **116**, 63–68.